ELSEVIER

Atmospheric Environment 38 (2004) 6999–7008

ATMOSPHERIC ENVIRONMENT

www.elsevier.com/locate/atmosenv

Detection of Asian dust aerosols using meteorological satellite data and suspended particulate matter concentrations

Naoko Iino[a,*], Kisei Kinoshita[b], Andrew C. Tupper[b,c], Toshiaki Yano[a]

[a]*Department of Mechanical Engineering, Kagoshima University, Kagoshima, Japan*
[b]*Physics Department, Faculty of Education, Kagoshima University, Kagoshima, Japan*
[c]*Bureau of Meteorology, Darwin, Australia*

Received 20 September 2003; received in revised form 13 February 2004; accepted 25 February 2004

Abstract

The advection and dispersion of Asian dust events from China to the Pacific Ocean around Japan during 2000–2002 were investigated using the meteorological satellite data of NOAA/AVHRR and GMS-5/VISSR. Aerosol vapour index images, taking the brightness temperature difference between 11 and 12 μm, are very effective for monitoring the Asian dust phenomenon in the East Asia region, with their capacity for detection during the day or night. We discuss the dust events, focusing on the advection patterns shown in satellite images, which are classified into three types as 'dry slot', 'high-pressure wedge' and 'travelling high', based on synoptic patterns. The results are compared with suspended particulate matter concentrations measured at Japanese surface stations and with ground-based observations of Sakurajima volcano by a web camera system at Kagoshima in Kyushu, Japan. We found that the passage of cold fronts caused a rapid increase of suspended particulate matter (SPM) concentrations, which exceeded $100\,\mu g\,m^{-3}$, and that deep low-pressure complexes strengthened the dust phenomenon. The 'high-pressure wedge' type is seen much more clearly in satellite images than the 'travelling high' type, but SPM concentrations and visibility were similar in both owing to the differences in the vertical distribution of the dust and in viewing conditions.
© 2004 Elsevier Ltd. All rights reserved.

Keywords: GMS/VISSR; NOAA/AVHRR; Split window method; Yellow sand; Suspended particulate matter; Web camera monitoring

1. Introduction

For the 3 years since 2000, the Asian dust phenomenon has been remarkable. Asian dust plays an important role in the climate and helps in examining atmospheric flows from East Asia to the northern Pacific Ocean, as a kind of tracer in the atmosphere. The dust storms originate from arid regions in China and Mongolia, such as the Takla Makan, Gobi, and Ordos deserts, and the Loess plateau. They are initiated by strong winds, caused by cold fronts or low-pressure systems. These dust phenomena are most frequently observed in Japan in the springtime, when the arid regions are covered with little snow or vegetation. Heavy dust events crossed the Pacific to affect North America, such as in April 1998 (Husar et al., 2001; Uno et al., 2001) and 2001 (Simpson et al., 2003). These events were discussed in detail by comparing satellite images, a regional-scale meteorological model (Uno et al., 2001), and ground observations exchanged through the Internet by the Asian Dust Network (Murayama et al., 2001).

*Corresponding author.
E-mail address: iino@mech.kagoshima-u.ac.jp (N. Iino).

1352-2310/$ - see front matter © 2004 Elsevier Ltd. All rights reserved.
doi:10.1016/j.atmosenv.2004.02.070

Similar dust storms associated with the El Niño-related drought were observed in Australia during the southern hemisphere spring and summer of 2002/2003.

We have analysed the advection and dispersion of Asian dust events from China to the Pacific Ocean around Japan since 1997, using Advanced Very High Resolution Radiometer (AVHRR) data from the NOAA polar orbiting satellites, and Visible and Spin-Scan Radiometer (VISSR) data from the fifth Japanese Geostationary Meteorological Satellite (GMS-5) (Kinoshita et al., 2001; Masumizu et al., 2002; Iino et al., 2003, 2004). In our satellite analysis, we take the brightness temperature difference between 11 and 12 μm bands. These images and related publications are displayed at our website at http://arist.edu.kagoshima-u.ac.jp/adust/kosa-e/kosa-e.htm. The images are very effective for distinguishing dust regions in dry air from water clouds and for monitoring dust in East Asia, because of the opposite properties of silicate dust particles, which are a major component of Asian dust, against water vapour at infrared wavelengths (Prata, 1989a, b) and of the capacity of infrared techniques to monitor the dust during the night.

Temperature difference images around Japan using Geostationary Meteorological Satellite data are displayed in real-time and archived at the website: Weather Home, Kochi University, http://weather.is.kochi-u.ac.jp/sat/gms.fe-sp/. The images are often used as 'quick look' images by Asian dust researchers, especially during the dust season. It is important to clarify the physical characteristics and observational limitations of Asian dust detected in the temperature difference imagery, to aid the use of this imagery in conjunction with numerical results and ground observations. Here we discuss the Asian dust storms during 2000–2002, focusing on the relation between the advection patterns shown in satellite images. They are classified into three types, based on synoptic patterns, and the typical scenes are discussed in conjunction with suspended particulate matter (SPM) concentrations at the ground surface and visual observations by a web camera system at Kagoshima in Kyushu, Japan. Information exchanged by the Asian Dust Network (AD-Net) during 2000–2002 is also used to confirm the transport paths and the vertical structures of dust and the observed phenomena at China, Korea and Japan.

2. Satellite detection of Asian dust and their advection patterns

2.1. Asian dust detection by brightness temperature differences of NOAA/AVHRR and GMS/VISSR

NOAA-16/AVHRR has six bands: visible, near-infrared, short-wave infrared, mid-infrared, and two thermal-infrared bands. GMS-5/VISSR has four bands: visible, and three thermal-infrared bands. Asian dust images of each band are shown and discussed in detail in Iino et al. (2003). Here, we concentrate our discussion only on Asian dust detection using the thermal-infrared bands AVHRR-4 (10.3–11.3 μm), AVHRR-5 (11.5–12.5 μm), VISSR-IR1 (10.5–11.5 μm) and VISSR-IR2 (11.5–12.5 μm).

Thermal-infrared images of 11 and 12 μm are similar and their single band images are not very sensitive to Asian dust. However, the difference of these split-window bands is very useful for detecting airborne silicate dust particles such as Asian dust (Kinoshita et al., 2001; Masumizu et al., 2002; Iino et al., 2003, 2004) and volcanic ash clouds (Prata, 1989a, b; Kinoshita et al., 1993). This algorithm is based on the split-window method that has developed to estimate water vapour amounts in the air (Inoue, 1990). The volcanic and silicate substances whose particle sizes are less than a wavelength have opposite extinctive properties to ice crystals and water droplets in 11 and 12 μm bands, an effect termed as 'reverse absorption' (Prata, 1989a, b). Asian dust is well detectable by temperature difference images, because the algorithm assumption by Prata (1989a, b), a plane-parallel semi transparent plume layer with homogeneous physical properties, more closely matches the Asian dust distributions than volcanic plumes (Simpson et al., 2003). Therefore, the difference of these bands can be used to evaluate the competing effects of the silicate dust particles and of water and ice. Sokolik (2002) gives details of dust absorption characteristics for various atmospheric dust loadings, compositions, and wavelengths and satellite sensors.

We calculate the brightness temperature difference of 11 and 12 μm bands as the Aerosol Vapour Index (AVI) by the following equations:

$$\mathrm{AVI(AVHRR)} = n(5) - n(4) + 200, \quad \text{for NOAA/AVHRR},$$

$$\mathrm{AVI(VISSR)} = \mathrm{IR}(2) - \mathrm{IR}(1) + 100, \quad \text{for GMS-5/VISSR},$$

where, $n(i)$ and $\mathrm{IR}(i)$ of thermal-infrared band i correspond to the brightness temperature $t(i)$ and $T(i)$ in centigrade as $t(i) = 0.1n(i) - 50$, for $i = 4, 5$, and as $T(i) = 0.5\mathrm{IR}(i) - 85$, for $i = 1, 2$, respectively. Here the term 'aerosol' means silicate dust particles suspended in the atmosphere. In the definition of AVI, the subtraction of 11 μm band from 12 μm band is done, so as to enhance the dust region as a bright area (with higher AVI value), and a positive constant is added in order to avoid negative quantities for convenience. The constants of 200 or 100 are selected according to the raw data format; 10-bit for NOAA/AVHRR or 8-bit for GMS/VISSR, respectively. In monochrome AVI images, the dense Asian dust is bright and the more dispersed

regions are relatively bright compared with the surroundings. By contrast, regions with moist air are relatively dark. As mentioned above, the signal of dispersed Asian dust is partly cancelled by the water vapour effect, but still keeping a relatively higher value than surroundings with no dust. Iino et al. (2001) examined the relation between the precipitable water amounts (PW) calculated from sounding data and the brightness temperature differences of AVHRR in 11 and 12 μm for light and moderate dust events observed around Japan in 1997 and 1998, respectively. In the moderate dust case, the brightness temperature difference values were lower (implying less water vapour in a clear sky) than the values in the case of light dust, though the actual PW values were larger than that of the light dust case. This suggested the competing effect between water vapour and dust loading. Sokolik (2002) demonstrated that the presence of dust decreases the brightness temperature across the infrared radiation region and that this spectral signature is independent of either the temperature profile or the amount of water vapour. Finally, it should be noted that it is impossible to detect the dust layers covered with thick clouds by satellite observations.

The NOAA/AVHRR 4 and 5 bands have higher temperature resolution, 0.1 K, than GMS-5/IR-1 and 2, 0.5 K, and have higher spatial resolution and spectral separations. Therefore, NOAA/AVHRR can detect thin dust layers in detail, while GMS/VISSR has less dust sensitivity. Tokuno (1997) and Merchant et al. (2003) clarified that the larger overlap of the 11 and 12 μm bands on GMS/VISSR compared to NOAA/AVHRR (Fig. 1) leads to less temperature difference. However, frequent observation, at an hourly interval, with a fixed view is of great advantage for monitoring of Asian dust, as for monitoring of volcanic clouds (Tokuno, 1997). The standard products of GMS-5/VISSR by the Japan Weather Association cover the range 100–180° E and 5S–60° N with an hourly interval. We analysed the area, illustrated in Fig. 2, covering 100–165 °E and 20–55 °N with 3 or 6 hourly intervals. Although the Takla Makan desert is out of the scope of these products, we can monitor the phenomena of Asian dust travelling from other source regions to the Pacific Ocean with high frequency and a fixed view.

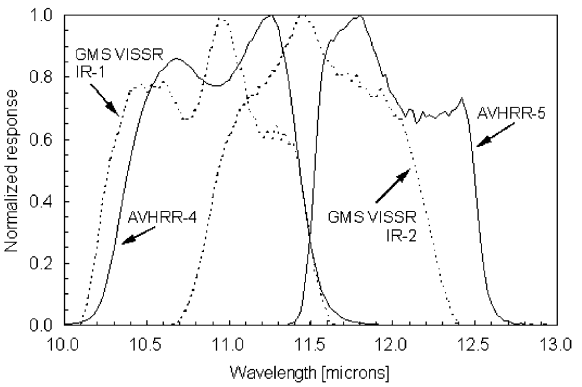

Fig. 1. Spectral response functions for the 11 and 12 μm bands for the GMS-5/VISSR (IR-1 and 2, respectively) and NOAA-16/AVHRR (bands 4 and 5, respectively).

2.2. Advection patterns of Asian dust

Asian dust events seen in satellite images are briefly summarized as follows. In the case of a dust event caused by a deep low-pressure system, we first observe the dense dust in the cloud-free area near the low, and then dispersed dust distributed in a mobile high-pressure system travelling from the west. Notable heavy dust phenomena are often associated with multiple low-pressure systems. In such cases, the dust in the area between the rear of a cold front and ahead of the following low is significantly denser than the dust in a mobile high.

Three types of advection patterns seen in AVI images are shown in Figs. 3a and b, and corresponding synoptic charts are Figs. 3c and d. In Fig. 3a, the dense dust region indicated by 'D' is seen in the rear of a cold front as a comma-shaped, cloud free region entraining into a developed low (at [50 °N, 125 °E] in Fig. 3c). We describe this pattern as a 'dry slot' type, which can also be seen in Figs. 4a–c, 5b, 6a and 7a. The dust particles descend toward the ground surface at the rear of a cold front as the region of strong frontal uplift passes; thus the SPM

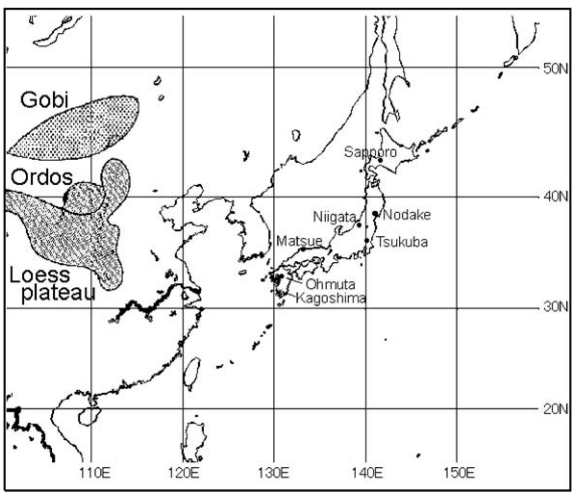

Fig. 2. The domain of GMS AVI imagery covering 100–165 °E and 20–55 °N, and the locations of the Gobi and Ordos deserts and the Loess plateau. The locations of the national environmental gas-monitoring stations in Japan are also shown, together with Kagoshima City in Kyushu, Japan.

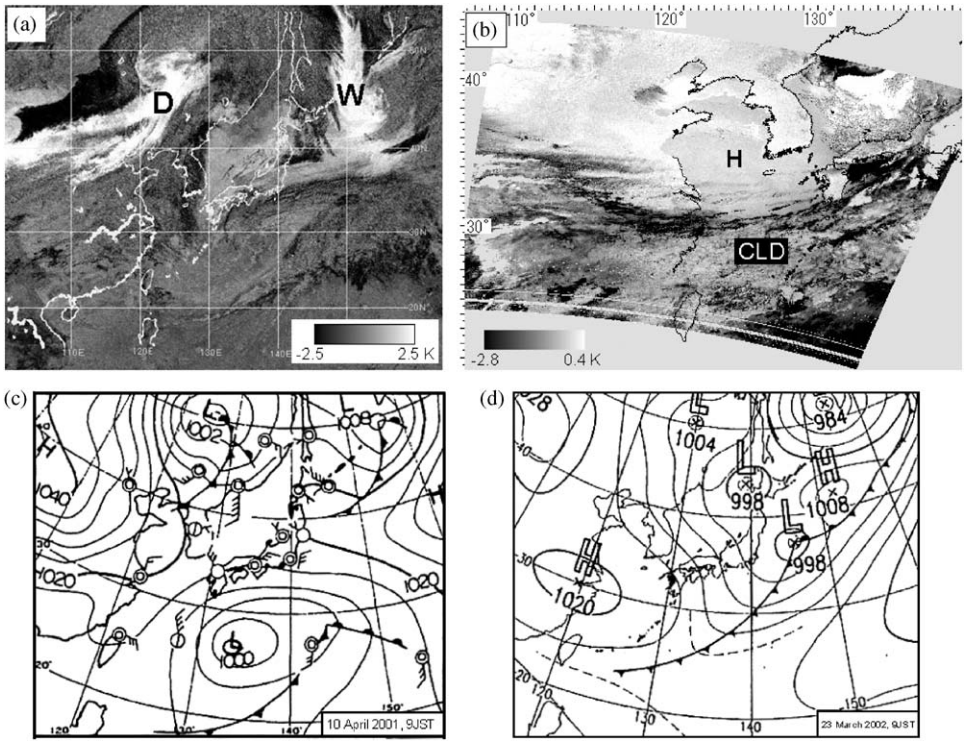

Fig. 3. Typical images of the three types of the advection patterns 'D', 'W' and 'H' indicate the 'dry slot', 'high-pressure wedge' and 'travelling high' types, respectively. (a) GMS AVI image on 10 April 2001 at 1200 JST (Japanese Standard Time = UTC + 9 h). (b) NOAA AVI image on 23 March 2002 at 0557 JST. The synoptic charts at 0900 JST on 10 April 2001 (c) and on 23 March 2002 (d).

concentrations at the surface suddenly increase strongly after the passing of the cold front.

The dust seems enhanced in the narrow ridge of high-pressure between two low-pressure systems ('W' around [40–55 °N, 150 °E] in Fig. 3a). We describe this pattern as a 'high-pressure wedge' type, which is also seen in Fig. 5b.

Fig. 3b shows the dispersed dust distribution of the 'travelling high' type, in the fine weather area associated with a mobile high-pressure system (at [30 °N, 120 °E] in Fig. 3d). A similar scene is seen in Fig. 6b. This type is observed as a final stage of a dust event.

For these 'high-pressure wedge' and 'travelling high' types, the subsiding air mass brings dust particles near the atmospheric boundary layer and dust layers are often observed at a few kilometer heights by lidar. The SPM concentrations increase at a moderate rate; the suspended particles in high-pressure region are probably smaller on average those at the rear of a cold front.

Note that thick clouds with high altitude tops are somewhat bright similar to diffused dust (e.g., 'CLD' in Fig. 3b) because these clouds can be regarded as blackbody, i.e., the brightness temperature difference becomes zero, and the column density of water vapour above them is negligible. Another reason for the same result is, for AVHRR data, poor calibration at low temperatures (Potts and Ebert, 1996). However, these clouds can be discriminated during the day by a composite colour image containing additional use of short-wave infrared band (Iino et al., 2003).

3. Ground observations

3.1. Continuous monitoring of suspended particulate matter

We used the SPM data observed by the national environmental gas-monitoring stations in Japan indicated by black dots in Fig. 2. We also used the same kind of data observed in Kagoshima by the Kagoshima City Office. We graphed hourly SPM concentrations from March to May during 2000–2002. For the data in April and May 2001 and from March to May 2002, we graphed data from two stations in Kagoshima in order to separate the effect of Sakurajima volcano. The emissions from Sakurajima are usually localized compared to Asian dust; thus the variations of SPM

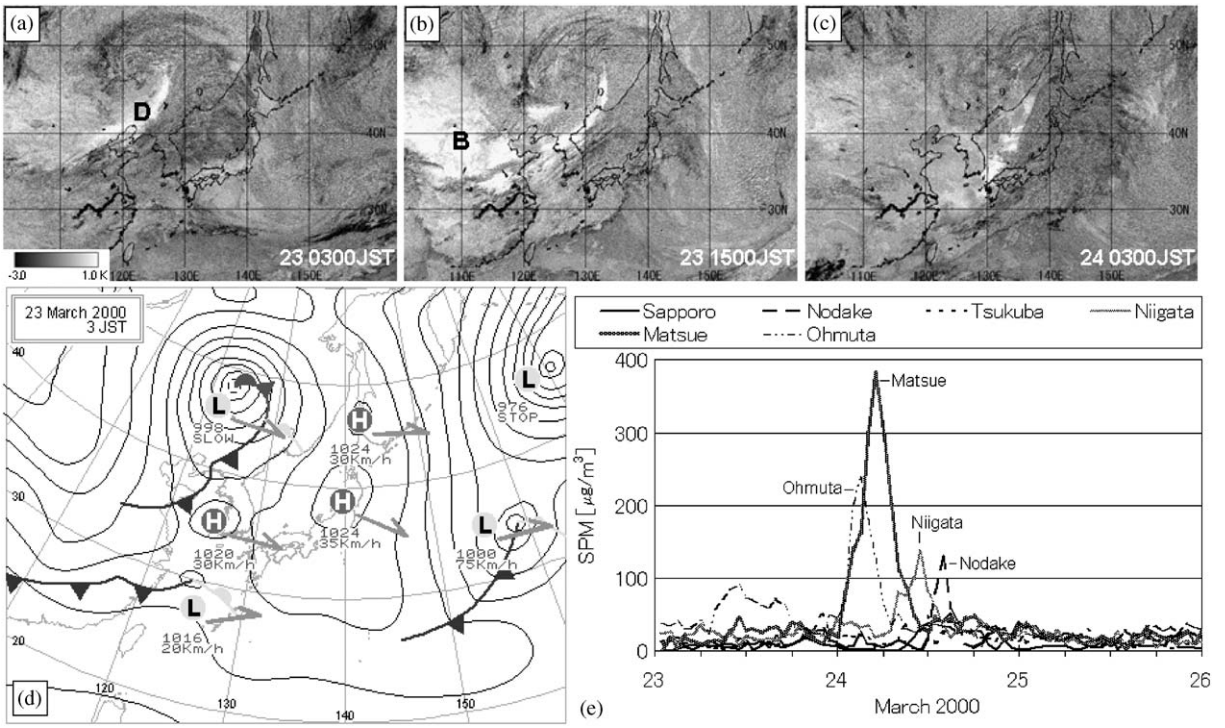

Fig. 4. (a)–(c) GMS AVI images at 12 hourly intervals from 0300 JST on 23 March 2000. 'D' and 'B' indicate the dust of 'dry slot' type and the bare surface area in the arid regions, respectively. (d) Synoptic chart at 0300 JST on 23 March 2000. (e) SPM concentrations at the national stations in Japan during 23–25 March 2000.

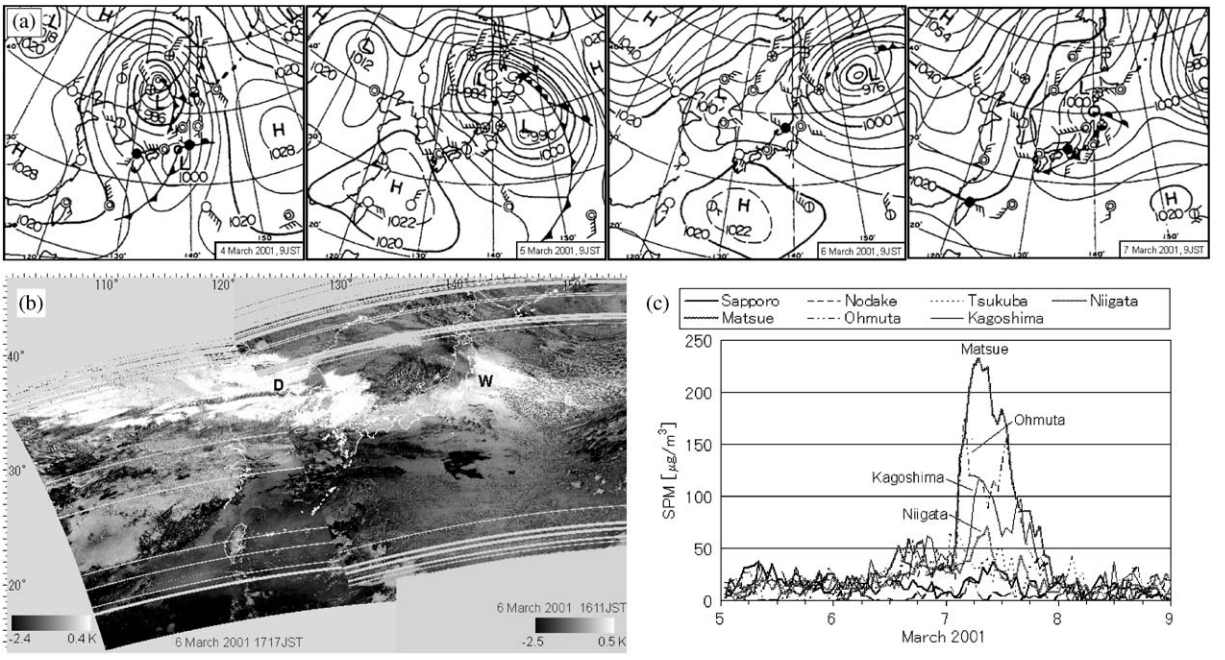

Fig. 5. (a) The synoptic charts at 0900 JST from 4 to 7 March 2001. (b) A NOAA AVI mosaic image at 1611 and 1717 JST on 6 March 2001. 'D' and 'W' indicate the 'dry slot' and 'high-pressure wedge' types, respectively. (c) The time variations of SPM concentrations at the national stations and Kagoshima during 5–8 March 2001.

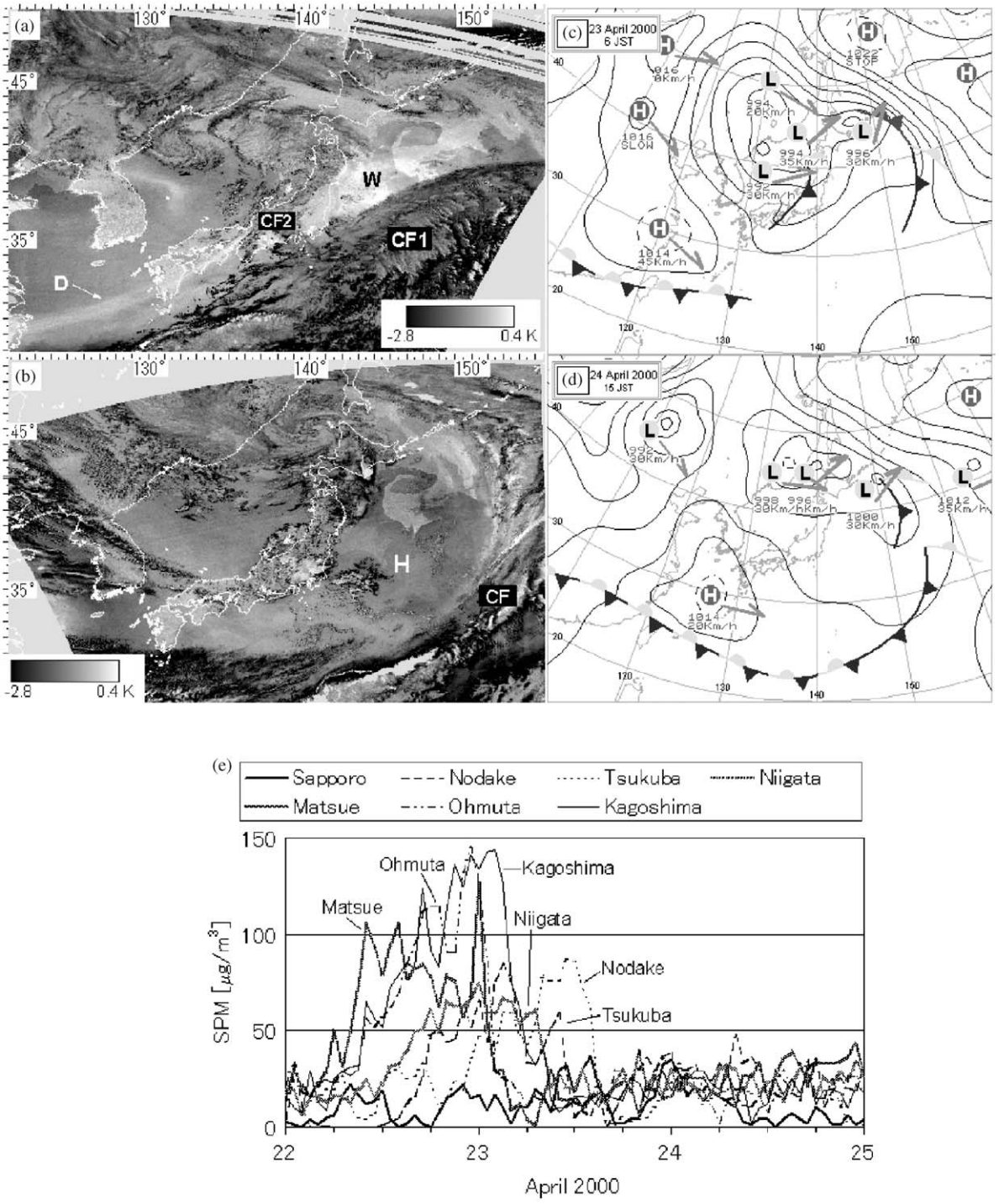

Fig. 6. NOAA AVI images at 0537 JST on 23 April 2000 (a) and at 1631 JST on 24 April 2000 (b). The dust areas of 'dry slot', 'high-pressure wedge' and 'travelling high' denoted as 'D', 'W' and 'H', respectively, and 'CF' which indicates a cold front. Synoptic charts at 0600 JST on 23 April 2000 (c) and at 1500 JST on the next day (d). (e) Same as Fig. 5(c) but during 22–24 April 2000.

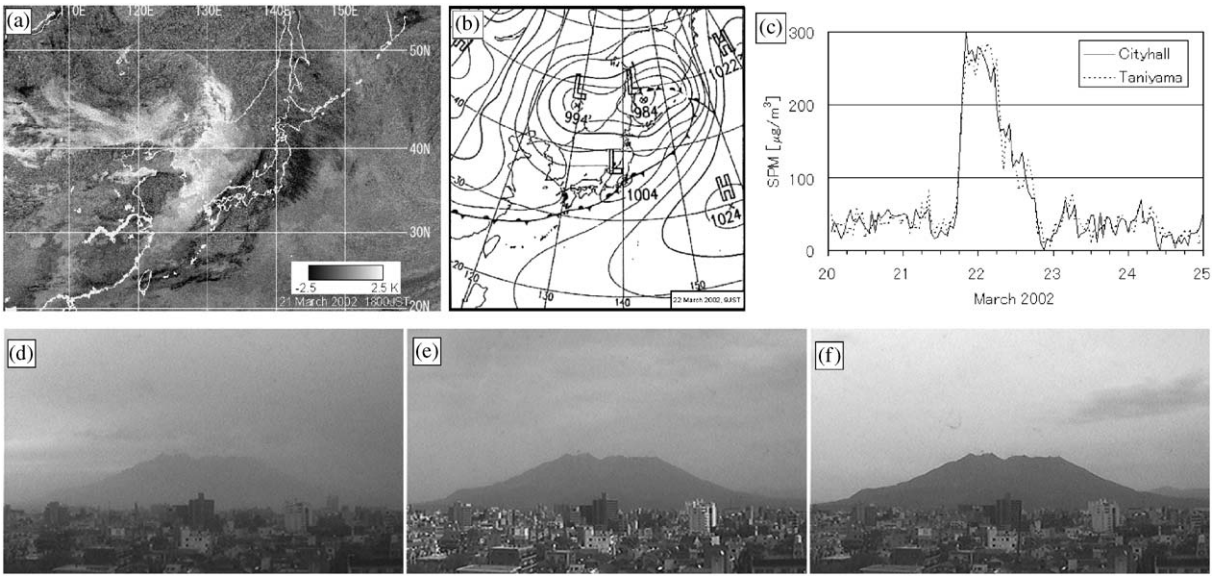

Fig. 7. (a) GMS AVI image at 1800 JST on 21 March 2002. (b) Synoptic chart at 0900 JST on 22 March 2002. (c) Temporal variations of SPM concentrations at the City Hall and Taniyama stations in Kagoshima during 20–24 March 2002. The images of Sakurajima volcano at 1000 JST on 22 (d), at 1300 JST on 23 (e) and at 1400 JST on 24 (f) in March 2002.

concentrations at multiple stations help to separate local effects.

3.2. Ground-based observations by a web camera at Kagoshima city

Mt. Sakurajima is one of the most active volcanoes in the world, situated about 10 km east of Kagoshima in Kyushu, Japan. In order to monitor the volcanic activities and investigate the plume behaviour, ground-based observations of the volcano have been performed since 1987 (Kinoshita, 1996; Kinoshita et al., 2003). Here, we use the images taken from one of the observation points using a web camera, located 10 km west of the crater, and the images taken at 5 min intervals have been archived and displayed at the following website: http://volceye.edu.kagoshima-u.ac.jp/webcam/archive/.

These images were useful not only for volcanic research but also for monitoring the Asian dust at Kagoshima. The decrease of visibility is obviously shown in the images. The dusty scenes were seen as a yellow coloration of the sky. The reduction of the blue component that separated from the colour images is larger compared to the other components, red and green, because of the preferential absorption of blue light. This is due to the optical properties of silicates that display an increasing absorption coefficient with decreasing wavelength from 300 to 700 nm (Patterson et al., 1977). Additional images taken from other sites help to distinguish Asian dust from volcanic effects.

4. Comparison with satellite images and other data

Typical cases of satellite images and the variations of SPM concentrations are shown in Figs. 4–7, and the web camera results are shown in Fig. 7. Related synoptic charts and the AD-Net information at the following website are also described: http://info.nies.go.jp:8094/AD-Net/index.html.

4.1. Dust phenomenon of 'dry slot' type by a deep low-pressure system

Figs. 4a–c are a time-series of GMS AVI images at twelve hourly intervals from 0300 JST (Japanese Standard Time = UTC + 9 h) on 23 March 2000. The 'dry slot' pattern of dense dust accompanying a deep low-pressure system was transported slowly eastwards. The synoptic chart at 0300 JST on 23 March is shown in Fig. 4d and the dense dust denoted as 'D' in Fig. 4a corresponds well to the location of a cold front. At Chongwon, Korea, peaks of total suspended particulate exceeding 1400 $\mu g\,m^{-3}$ were observed on this day. Dust was observed in Japan on 24 March. Simulation of this event (Kinoshita et al., 2001) suggests that, though the dust covered by cloud is not detectable by satellite, very high dust concentrations are seen in the cloud-free, 'dry slot' region. The time variation of SPM concentrations at the national stations during 23–25 March 2000 are illustrated in Fig. 4e. The sharp peaks from the left indicate SPM concentrations of 239, 381, 136 and 130 $\mu g\,m^{-3}$ at 0300, 0500, 1100 and 1400 JST in

Ohmuta, Matsue, Niigata and Nodake, respectively. The peak-time at each station corresponds well with the transport of the dust from the west to the east.

We should note that bare surfaces in arid regions, under fine weather, have similar AVI values to dense dust areas owing to the difference of the emissivities in the 11 and 12 μm region (Fig. 4b, 'B'). Although it is difficult to distinguish between dust and bare surfaces by using infrared satellite data only, the fact that the brightness temperature of semi-transparent dust clouds at 11 or 12 μm is lower than the surface temperature, and the obvious differences between the mobile dust clouds and the static land surfaces on animated imagery help to avoid misclassification. The views of the detailed textures of the land surface and topographic features, such as the Yellow River, can be used to help identify false alarms by diagnosing clear-air situations.

4.2. Dust phenomena of 'high-pressure wedge' type and the following 'dry slot' type

The synoptic patterns during 4–7 March 2001 around Japan were as follows (Fig. 5a). A low-pressure system developed on 4 March 2001 in the Maritime Provinces in Russia, and travelled eastwards to be located east of Hokkaido on 6 March. The following low, which moved over the Gobi, Ordos and Loess plateau areas, was accompanied by dust, and was located on the Korean peninsula on 6 March and then crossed over the Japanese islands on 7 March. Iino et al. (2004) demonstrated the dust event for this period using the temporal GMS AVI images, and they corresponded well to the simulation results of aerosol optical thickness of dust.

Fig. 5b is a mosaic NOAA AVI image at 1611 and 1717 JST on 6 March 2001, and Fig. 5c illustrates the SPM concentrations during 5–8 March 2001. The dust labelled 'W' in Fig. 5b is in the area between the rear of a developed low and ahead of the following low. The dust layers existed up to 7 km in Tokyo at 12 JST on 6 March. In the AVI imagery, the dust of 'high-pressure wedge' type is displayed as an enhanced dust area, whereas the increases of the SPM concentrations are unremarkable, about 50–60 $\mu g\,m^{-3}$. The rapid increases of SPM concentrations from 0300 JST on 7 March were caused by dust in the somewhat diffused 'dry slot' pattern shown in Fig. 5b as 'D'. This is supported by the lidar observation that two dust layers were at the altitude of around 3 km in Tokyo at 21 JST on 6 March.

4.3. Dust phenomena by multiple low-pressure systems

Figs. 6a and b are NOAA AVI images at 0537 JST on 23 April 2000 and at 1631 JST on the next day, respectively. The synoptic charts are shown in Figs. 6c and d and the SPM concentrations during 22–24 April are shown in Fig. 6e. From 22 to 23 April, the low-pressure complexes moved slowly around 40–50 °N, and brought dust over Japan. The dust plume, denoted as 'D', is seen behind a cold front located on the Japanese islands, and the dust region of 'high-pressure wedge' type (denoted as 'W') is also shown in Fig. 6a. The dispersed dust distribution in a mobile high-pressure system extending over western Japan is seen in Fig. 6b.

The first remarkable increases of SPM concentrations from 1000 JST on 22 April to 0300 JST on 23 April 2000 were caused by the passing of a cold front, denoted as 'CF1' in Fig. 6a. The second smaller peaks of SPM concentrations were observed in the morning on 23 April. These were 61 $\mu g\,m^{-3}$ at 0700 JST in Niigata, 59 $\mu g\,m^{-3}$ at 1000 JST in Nodake, and 88 $\mu g\,m^{-3}$ at 1100 JST in Tsukuba. These peaks correspond to the crossing of the cold front denoted as 'CF2' in Fig. 6a. As shown in Fig. 6e, the dust events owing to the multiple low-pressure systems continued longer than the event caused by a single low. A mobile high became dominant over Japan (except in the north, over Hokkaido) from the afternoon on 23 April, and the SPM concentrations maintained a lower level, less than 50 $\mu g\,m^{-3}$.

4.4. Visibility and SPM concentrations during dust phenomena

Fig. 7a shows a GMS AVI image at 1800 JST on 21 March 2002. The dust of 'dry slot' type is seen over Kyushu, behind a cold front. The synoptic chart at 0900 JST on the next day is shown in Fig. 7b. Fig. 7c shows the SPM concentrations during 20–24 March 2002, monitored at two stations, the City Hall and Taniyama, 9 km apart in Kagoshima. SPM concentrations at both stations exceeded 100 $\mu g\,m^{-3}$ at 1800 JST on 21 March, with values of 122 and 125 $\mu g\,m^{-3}$, respectively. This was one of the heaviest events in 3 years. It caused serious disruption of traffic in Korea and Japan, and elementary schools and kindergartens were all closed in Korea. Iino et al. (2003) described the overall event using the temporal GMS AVI images and AD-Net information. The event was a 'dry slot' type and an enhanced 'high-pressure wedge' type, associated with a deep low-pressure complex passing near Hokkaido and with a stationary front located near the southern coast of the Japanese islands (see Fig. 7b). Fig. 7d is an image of Sakurajima volcano at 1000 JST on 22 March 2002, with SPM concentrations of 175 and 150 $\mu g\,m^{-3}$at the City Hall and Taniyama, respectively. The visibility observed by the Kagoshima Local Meteorological Observatory (KMO) was 8 km at 0900 JST. These high concentrations continued for 24 h, and SPM concentrations then decreased due to rain around midnight (Fig. 7c).

Dust of the 'travelling high' type was seen in the satellite images of 23 March, and SPM concentrations

were maintained at about 40 $\mu g\,m^{-3}$. Fig. 7e shows an image at 1300 JST on 23 March. The visibility at the KMO was 12 km at 1200 JST, and the SPM concentrations were 48 and 28 $\mu g\,m^{-3}$ at the City Hall and Taniyama. Finally, we show an example of clear conditions. Fig. 7f illustrates an image of Mt. Sakurajima at 1400 JST on 24 March. The visibility at 1500 JST was recorded as 40 km by KMO. SPM concentrations at the City Hall and Taniyama stations were 22 and 17 $\mu g\,m^{-3}$, respectively.

5. Concluding remarks

The Asian dust phenomenon during 2000–2002 was investigated focusing on the relation between the three types of the advection patterns shown in the satellite images and the SPM concentrations at the ground surface, in conjunction with ground observations. The physical characteristics and observational limitations of Asian dust detected in the temperature difference imagery were described in detail and advection patterns were classified into the 'dry slot' type, 'high-pressure wedge' type and 'travelling high' type.

Rapid increases of SPM concentrations to values exceeding 100 $\mu g\,m^{-3}$ in Japan were caused by cold front passages. The dense dust as clearly seen in satellite images as 'dry slot' type. Deep low-pressure complexes enhance the dust phenomena, making high SPM concentrations last longer than events due to a single low-pressure system. For the forecasting of heavy dust phenomena, we may focus on the movement of the cold front(s) associated with the low, and in addition, the existence of any stationary front associated with convergence zones should be noted.

In contrast, 'high-pressure wedge' patterns were shown as dense dust areas in satellite images, but increases of SPM concentrations were not as significant as the 'dry slot' type, and the 'high-pressure' type showed some smaller SPM concentrations. The difference of the characteristics of SPM concentrations between 'dry slot' type and others may be caused by the vertical structure of the dust owing to the meteorological conditions and the difference in the particle size distributions owing to the dry/wet depositions throughout the transport. Cool, subsiding air in the 'dry slot' region of a cold front concentrates dust near the surface, while dust associated with a high-pressure system may be more evenly distributed in layers in the lower troposphere. In both cases, dust is more visible in satellite imagery than in surrounding areas of uplift and higher moisture, because dust signals are partially masked by moisture and completely obscured by cloud.

The ground-based visual observations of Sakurajima volcano at Kagoshima in Kyushu, Japan, were consistent with SPM concentrations and visibilities observed by Kagoshima Local Meteorological Observatory. This suggests the possibility of quantitative investigation for the Asian dust phenomena using automatic monitoring images. Detailed studies of the colour composite analysis of dust images will be done in the near future.

Acknowledgements

The synoptic charts in Figs. 3, 5 and 7 and Figs. 4 and 6 were provided by the Japan Meteorological Agency and Japan Weather Association, respectively. We are indebted to Professor T. Masumizu of the Daiichi Welfare University, and to Mr. R. Iwasaki and Ms. M. Koyamada of the Faculty of Education, Kagoshima University, for extensive analysis of the satellite data and discussions. We are grateful to the members of AD-Net for on-line information. We thank the Kagoshima City Office for providing the gas-monitoring data in Kagoshima, and the administration committee of the satellite data station in Kagoshima University for the on-line use of NOAA/AVHRR data. We also thank the anonymous referees for helpful suggestions and comments.

References

Husar, R.B., Tratt, D.M., Schichtel, B.A., Falke, S.R., Li, F., Jaffe, D., Gasso, S., Gill, T., Laulainen, N.S., Lu, F., Reheis, M.C., Chun, Y., Westphal, D., Holben, B.N., Gueymard, C., McKendry, I., Kuring, N., Feldman, G.C., McClain, C., Frouin, R.J., Merrill, J., DuBois, D., Vignola, F., Murayama, T., Nickovic, S., Wilson, W.E., Sassen, K., Sugimoto, N., Malm, W.C., 2001. Asian dust events of April 1998. Journal of Geophysical Research 106 (D16), 18317–18330.

Iino, N., Kikukawa, H., Kinoshita, K., Yano, T., 2001. Relationship between perceptible water amount obtained from upper air data and AVHRR split window measurement in Asian dust season—case studies in April of 1997 and 1998—(in Japanese with English abstract). Proceedings of the 31st conference Remote Sensors Society Japan, pp. 59–62.

Iino, N., Kinoshita, K., Iwasaki, R., Masumizu, T., Yano, T., 2003. NOAA and GMS observations of Asian dust events during 2000–2002. In: Menzel, W.P., Zhang, W.J., Marshall, J.L., Tokuno, M. (Eds.), Proceedings of SPIE, vol. 4895, Applications with Weather Satellites. SPIE, Bellingham, WA, USA, pp. 18–27.

Iino, N. Masumizu, T., Kinoshita, K., Uno, I., Yano, T., Torii, S., 2004. Temporal behavior of Asian dust aerosols observed in 2001 using meteorological satellite data. International Journal of Environmental Technology and Management, in press.

Inoue, T., 1990. The relationship of sea surface temperature and water vapor amount to convection over the western tropical

pacific revealed from split window measurements. Journal of Meteorological Society Japan 68 (5), 589–606.

Kinoshita, K., Hosoyamada, S., Goto, A., Saitoh, S., 1993. NOAA-AVHRR imagery of volcanic clouds in Kyushu, Japan. Proceedings of the International Geoscience and Remote Sensing Symposium. Tokyo, Japan, pp. 1824–1826.

Kinoshita, K., 1996. Observation of flow and dispersion of volcanic clouds from Mt. Sakurajima. Jounal of Atmospheric Environment 30 (16), 2831–2837.

Kinoshita, K., Iwasaki, R., Koyamada, M., Iino, N., Yano, T., Uno, I., Amano, H., Yoshii, H., Masumizu, T., 2001. Observation of Asian dusts during 1997–2000 by NOAA/AVHRR. In: Takeuchi, N., Kuze, H., Takamura, T. (Eds.), Proceedings of the CEReS International Symposium Remote Sensing of the Atmosphere and Validation of Satellite Data. Chiba University, Chiba, Japan, pp. 7–12.

Kinoshita, K., Kanagaki, C., Tupper, A.C. and Iino, N., 2003. Observation and analysis of plumes and gas from volcanic islands in Japan. In: Manfrida, G., Contini, D. (Eds.), Proceedings of the International Workshop on Physical Modeling of Flow and Dispersion Phenomena. Firenze University Press, pp. 78–83.

Merchant, C.J., Simpson, J.J., Harris, A.R., 2003. A cross-calibration of GMS-5 thermal channels against ATSR-2. Remote Sensing Environment 84, 268–282.

Masumizu, T., Kinoshita, K., Yano, T., Torii, S., Iino, N., Uno, I., 2002. Analysis of advection and dispersion of Asian dusts using meteorological satellite data. In: Dost, S., Struchtrup, H., Dincer, I. (Eds.), Progress in Transport Phenomena—The 13th International Symposium on Transport Phenomena, Elsevier, pp. 803–808.

Murayama, T., Sugimoto, N., Uno, I., Kinoshita, K., Aoki, K., Hagiwara, N., Liu, Z., Matsui, I., Sakai, T., Shibata, T., Arao, K., Sohn, B.J., Won, J.G., Yoon, S.C., Li, T., Zhou, J., Hu, H., Abo, M., Iokibe, K., Koga, R., Iwasaka, Y., 2001. Ground-based network observation of Asian dust events of April 1998 in East Asia. Journal of Geophysical Research 106 (D16), 18345–18359.

Patterson, E.M., Gillette, D.A., Stockton, B.H., 1977. Complex index of refraction between 300 and 700 nm for Saharan aerosols. Journal of Geophysical Research 82 (21), 3153–3160.

Potts, R.J., Ebert, E.E., 1996. On the detection of volcanic ash in NOAA AVHRR infrared satellite imagery. 8th Australasian Remote Sensing Conference, Canberra, 25–29 March 1996.

Prata, A.J., 1989a. Infrared radiative transfer calculations for volcanic ash clouds. Geophysical Research Letters 16 (11), 1293–1296.

Prata, A.J., 1989b. Observations of volcanic ash clouds in the 10–12 μm window using AVHRR/2 data. International Journal Remote Sensors 10 (4), 751–761.

Simpson, J.J., Hufford, G.L., Servranckx, R., Berg, J., Pieri, D., 2003. Airborne asian dust: case study of long-range transport and implications for the detection of volcanic ash. Weather and Forecasting of the American Meteorological Society 18 (2), 121–141.

Sokolik, I.N., 2002. The spectral radiative signature of wind-blown mineral dust: Implications for remote sensing in the thermal IR region. Geophysical Research Letters 29 (24), 2154–2157.

Tokuno, M., 1997. Satellite observation of volcanic ash clouds, Japan Meteorological Satellite Center, Meteorological Satellite Center Technical Note 33, pp. 29–48.

Uno, I., Amano, H., Emori, S., Kinoshita, K., Matsui, I., Sugimoto, N., 2001. Trans-Pacific yellow sand transport observed in April 1998: A numerical simulation. Journal of Geophysical Research 106 (D16), 18331–18344.